JOURNAL OF GEOPHYSICAL RESEARCH, VOL. 101, NO. A12, PAGES 27,251–27,269, DECEMBER 1, 1996

Simulation of pressure pulses in the bow shock and magnetosheath driven by variations in interplanetary magnetic field direction

Y. Lin, [1] D. W. Swift, [2] and L. C. Lee [3]

Abstract. Two-dimensional (2-D) hybrid simulations are carried out to study the effects of the variation in the interplanetary magnetic field (IMF) direction on the bow shock, magnetosheath, and magnetosphere. A curvilinear coordinate system is used in the simulation. The 2-D simulation is also compared with our one-dimensional simulation results. It is found that pressure pulses are generated as a result of the interaction between the bow shock (BS) and an interplanetary rotational discontinuity (RD). First, a structure consisting of a rotational discontinuity and two slow shocks are present downstream of the bow shock after the BS/RD interaction. The magnetic field and plasma density are anticorrelated in this structure. The dynamic pressure increases in the structure, leading to a pressure pulse in the magnetosheath. Second, a pressure pulse associated with reflected ions at the bow shock may be generated in the foreshock when the IMF changes its direction, especially when a local quasi-parallel bow shock becomes a quasi-perpendicular shock. The magnetic field, plasma density, and dynamic pressure are positively correlated in the upstream pressure pulse. This pressure pulse convects through and interacts with the bow shock, producing a pressure pulse in the downstream region. The downstream pressure pulses propagate to the magnetopause. The amplitude of the downstream pressure pulses can be up to 100% of the background magnetosheath value. It is suggested that the pressure pulses impinging on the magnetopause may lead to the magnetic impulse events observed in the high-latitude ionosphere.

1. Introduction

As the supersonic solar wind flows past the Earth, a fast shock that stands against the solar wind is produced; this shock is referred to as the bow shock [e.g., *Cahill and Patel*, 1967]. Downstream of the bow shock the magnetic field, plasma density, and pressure increase from their values in the solar wind, forming the magnetosheath region surrounding the Earth's magnetosphere. The solar wind is slowed and deflected in the magnetosheath. A systematic study of the position and shape of the curved bow shock front and the properties of flow around the magnetosphere has been conducted by using a gasdynamic-frozen field MHD theory [e.g., *Spreiter and Stahara*, 1985]. Near the magnetopause the magnetic flux piles up, resulting in the existence of a plasma depletion layer [*Lees*, 1964; *Zwan and Wolf*, 1976; *Crooker at el.*, 1979]. In addition, slow mode structures are observed in the magnetosheath [e.g., *Song et al.*, 1992], in which the magnetic field decreases and plasma density increases.

Mass, energy, and momentum are transferred to the magnetopause at interface between the magnetosheath and the geomagnetic field. A variety of transient physical processes may occur at the magnetopause, including bursty magnetic reconnection resulting in flux transfer events (FTEs) [*Russell and Elphic*, 1978] and riplets on the magnetopause driven by solar wind dynamic pressure pulses [*Kaufmann and Konradi*, 1969]. Since the magnetic field lines in the outer dayside magnetosphere are anchored in the high-latitude ionosphere, one might expect ground magnetometers to observe corresponding transient events.

Magnetic impulse events (MIEs) have been observed by high-latitude ground magnetometers [*Lanzerotti et al.*, 1986, 1987; *Lanzerotti*, 1989; *Glassmeier et al.*, 1989]. In the events the magnetic field has isolated large-amplitude perturbations accompanied by impulsive perturbations in the ionospheric electric field [*Bering et al.*, 1988]. These MIEs are associated with antisunward moving traveling convection vortices observed by multiple stations [*Friis-Christensen et al.*, 1988]. Observations [*Friis-Christensen et al.*, 1988; *Sibeck et al.*,

[1]Physics Department, Auburn University, Auburn, Alabama.

[2]Geophysical Institute and Department of Physics, University of Alaska, Fairbanks, Alaska.

[3]Department of Earth Science, National Cheng Kung University, Tainan, Taiwan.

Paper number 96JA02733.
0148-0227/96/96JA-02733$09.00

1989; *Farrugia et al.*, 1989] and theories [e.g., *Southwood and Kivelson*, 1990; *Glassmeier and Heppner*, 1992; *Lysak et al.*, 1994] suggest that the events are related to changes in the intrinsic solar wind dynamic pressure and/or interplanetary magnetic field (IMF) orientation. A statistical study by *Konik et al.* [1994] shows that 50-70% of the MIEs are associated with substantial variations in the solar wind magnetic field direction (variations in B_y and B_z), while only 15-30% of the events are accompanied by changes in the solar wind dynamic pressure. *Bering et al.* [1990] reported several MIEs in which the IMF direction changes greatly, whereas the solar wind dynamic pressure and magnetic field strength remain nearly constant.

One-dimensional (1-D) MHD and hybrid simulations have been carried out to explore the possibility that a significant dynamic pressure pulse can be generated at the magnetopause by a change in the interplanetary magnetic field orientation striking the bow shock [*Lin et al.*, 1996; *Yan and Lee*, 1996]. The idea is that if the magnetic impulse events are caused by pressure changes applied to the magnetosphere, such changes must be generated at the bow shock or in the magnetosheath. In these studies, the interaction of an interplanetary rotational discontinuity (RD) or an Alfven wave with an initial bow shock (BS) is investigated. As a result of the BS/RD interaction, a large rotational discontinuity and two slow shocks are generated downstream of the bow shock, propagating toward the magnetopause. A pulse in plasma dynamic pressure ρV^2 is found to form in the region of these discontinuities. The dynamic pressure pulse causes the the total pressure $(P + B^2/2\mu_0 + \rho V^2)$ to increase by up to 100% of the background value in the magnetosheath. The pressure pulse propagates with a nearly constant amplitude [*Lin et al.*, 1996]. It is speculated that the pressure pulses impinging on the magnetopause may cause an inward and outward motion of the magnetopause and lead to the observed traveling convection vortices and MIEs. The transmission of Alfven waves through the bow shock has also been studied by using an ideal MHD analysis [*Hassam*, 1978].

Two-dimensional (2-D) MHD simulations have also been performed to study the interaction between the bow shock and interplanetary discontinuities and waves [*Yan and Lee*, 1994]. The study suggests that slow mode structures may be generated in the magnetosheath by such an interaction. The dynamic pressure pulses, however, are not examined in the study. Note that other mechanisms have also been suggested for the generation of slow mode and mirror mode structures in the magnetosheath [e.g., *Lee et al.*, 1991; *Southwood and Kivelson*, 1992; *Denton et al.*, 1995].

On the other hand, the interaction between upstream hydromagnetic waves and the bow shock has been investigated by using MHD [*McKenzie and Westphal*, 1970]. *Wu et al.* [1993] carried out 1-D MHD simulations to show that the interaction between an interplanetary tangential discontinuity and the bow shock can generate a fast wave in the downstream region. The interaction between a tangential discontinuity and a fast wave has also been studied by 1-D hybrid simulations [*Mandt and Lee*, 1991]. *Thomas et al.* [1991] carried out a 2-D hybrid simulation for the interaction of a planar bow shock with current sheets embedded in the upstream flow. The local disruption of the shock and the formation of hot flow anomalies are found in their simulation.

In addition, the structure of the collisionless bow shock itself often exhibits turbulence [e.g., *Greenstadt and Fredricks*, 1979]. Hybrid simulations show that quasi-parallel shocks, in which the shock normal angle θ_{Bn} is smaller than 45^o, have a structure very different from that of quasi-perpendicular shocks with $\theta_{Bn} > 45^o$ [e.g., *Leroy et al.*, 1982; *Kan and Swift*, 1983; *Leroy and Winske*, 1983; *Burgess*,1989; *Lyu and Kan*, 1990; *Scholer and Terasawa*, 1990; *Krauss-Varban and Omidi*, 1991]. Generally speaking, in a collisionless plasma, ion reflection at a fast shock plays an important role in the dissipation mechanism of supercritical fast shocks, in which the Alfven much number M_A of the shock is greater than a critical number of ~2 to 3. Counterstreaming ion beams may be present upstream of the quasi-parallel bow shock and may generate long-wavelength MHD turbulence in the upstream region, which may propagate back through the bow shock. A recent 1-D hybrid simulation by *Thomas et al.* [1995] also shows that upstream waves of quasi-parallel shocks can propagate through the bow shock and generate a small pressure pulse in the downstream region.

The purpose of this paper is to extend to two dimensions our 1-D simulations [*Lin et al.*, 1996] for the generation of pressure pulses by the BS/RD interaction. In addition to the pressure pulse generated at the downstream rotational discontinuity and slow shock as suggested by the 1-D study, we show that the reflected ions at the bow shock also produce a significant pressure pulse in the magnetosheath after the IMF changes its orientation. The variation of the IMF direction may cause the reflected ions to return to the 2-D curved bow shock at a position with a different local shock normal angle and Mach number and thus to generate a pressure pulse in the foreshock. These upstream pressure pulses may then propagate to and interact with the bow shock and produce a large-amplitude pressure pulse in the downstream. These effects of reflected ions have not been studied in our 1-D models. Satellite observations have shown that many of the observed pressure pulses upstream of the bow shock are generated near the bow shock and usually have positively correlated variations in magnetic field and plasma density, and these upstream dynamic pressure pulses correspond to compressions or rarefactions in the dayside magnetospheric magnetic field [*Fairfield et al.*, 1990]. The field and density are, however, anticorrelated at the pressure pulses which arise intrinsically in the upstream solar wind. The upstream pressure pulses examined by *Fairfield et al.* [1990] have a duration of a few minutes to 10 minutes, and some of them tend to be associated with IMF direction changes that cause a reconfiguration of the foreshock.

In this paper we present for the first time 2-D hybrid simulations for the interaction between an interplanetary rotational discontinuity and the bow shock. A

curvilinear coordinate system is used in the simulation. Our 1-D simulations [*Lin et al.*, 1996] for the BS/RD interaction are also briefly presented for comparison. The models used in this study are described in section 2. The simulation results are given in sections 3 and 4. Finally, a summary is given in section 5.

2. Models of the Study

The 2-D ($\partial/\partial z = 0$) simulation is carried out in the geomagnetic equatorial plane, in which the x axis is assumed to be along the Sun-Earth line and pointing to the Sun and the y axis is pointing from dusk to dawn. A curvilinear coordinate system is used in the simulation; this system consists of the radial distance r in the xy plane, the z axis pointing from north to south, and the polar angle $\theta \equiv \tan^{-1}(x/y)$. The Earth is located at the origin. Figure 1 shows this coordinate system. The simulation domain is within the region with $10\ R_E < r < 35\ R_E$ and $0^o \le \theta \le 180^o$. The inner boundary at $r = 10\ R_E$ corresponds to the magnetopause.

The 2-D hybrid code adapted in this study was developed by *Swift* [1995, 1996], who used a curvilinear coordinate system to model the Earth's magnetosphere on a global scale. Among other results the formation of the bow shock in front of the magnetosphere is shown in his study. In the hybrid code the ions are treated as discrete particles, and the electrons are treated as a massless fluid. The electrons are assumed to flow along magnetic field lines in a way that guarantees quasi charge neutrality. In our simulation the grids are uniformly distributed in the r and θ directions, with a total of 151×122 grids. The grid size along the r direction is $\Delta r = 0.17\ R_E$.

The ion gyrofrequency Ω_0 in the solar wind is chosen to be $0.5\ s^{-1}$, where $\Omega_0 = eB_0/mc$, B_0 is the magnitude of the IMF, e is the electron charge, m is the ion mass, and c is the speed of light. This value of Ω_0 corresponds to an IMF $B_0 \sim 5$ nT. In the solar wind the number of ion particles per R_E^2 is chosen to be $N_0 = 670$, and the ion inertial length $\lambda_0 = c/\omega_{pi0}$, where ω_{pi0} is the ion plasma frequency, is chosen to be $0.17\ R_E$. The Alfven speed in the solar wind is $V_{A0} = 0.084\ R_E s^{-1}$. The ion plasma beta β_0 is chosen to be 0.5, and the ion gyroradius is about $0.12\ R_E$ in the solar wind.

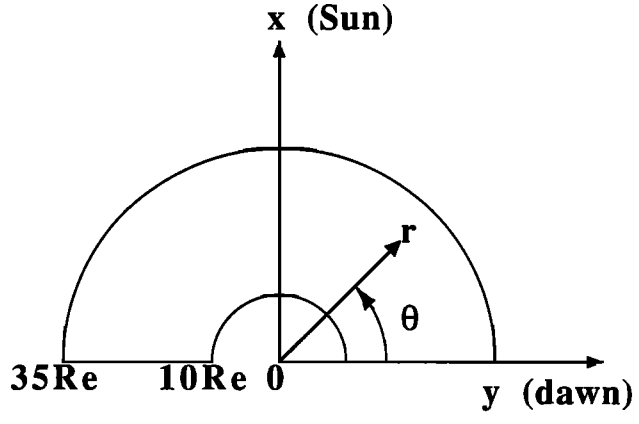

Figure 1. The curvilinear coordinate system used in the simulation, which consists of the radial coordinate **r** in the geomagnetic equatorial (xy) plane, the north-south direction z, and the polar angle θ. The x direction points to the Sun, and the y direction points to the dawn. The boundary at $r = 10\ R_E$ represents the magnetopause. The solar wind convects the IMF into the domain from the front side boundary at $r = 35 R_e$. The straight line boundary segments at $\theta = 0^o$ and $\theta = 180^o$ are two outflow boundaries.

The above value of the ion inertial length is about 10 times the real value in the solar wind, and the Alfven speed is about 7 times the real value. The reason for choosing a relatively large λ_0 in the simulation is as follows. The grid size along the normal of the bow shocks, which is nearly the r direction, must be smaller than the scale length of the shock, which is roughly of the order of a few ion inertial lengths. A small λ_0 will require a small Δr and thus more ion particles in the simulation, since the number of particles per cell must be greater than a few tens so that the code noise level is low. This approach will lead to a fairly long computing time. In our simulation a total of 1,900,000 particles are used, and the number of total time steps per run is nearly 1000. We have also run simulations for different λ_0 and have found that the position, shape, and strength of the bow shock are nearly unchanged. In addition, the choice of a large V_{A0} allows a large inflow velocity of the upstream solar wind for a given Alfven Mach number, and thus the simulation run can be completed in a shorter time. Note that the widths and speeds of discontinuities and the associated pressure pulses in the simulation, which will be discussed in the next section, are larger than those in the real magnetosheath.

The simulation is performed such that first, the bow shock BS is formed by the convection of high-speed solar wind along the $-x$ direction to the Earth, and second, the interplanetary rotational discontinuity RD is allowed to propagate into the domain toward BS at a certain time after the bow shock is formed. Initially, the solar wind is assumed to be uniform, and the IMF $\mathbf{B_0}$ is constant in the simulation domain. The ion temperature is assumed to be isotropic. At $t = 0$ the solar wind starts to pass the obstacle, i.e., the semicircular magnetopause. Across the front side boundary at $r = 35\ R_E$ the solar wind flows and convects the IMF $\mathbf{B_0}$ into the simulation domain. The straight line boundary segments at $\theta = 0^o$ and $\theta = 180^o$ represent two outflow boundaries.

There can be several choices for the boundary conditions at the magnetopause boundary, $r = 10\ R_E$. One choice is to set the normal magnetic field component to be zero there and to let the ions be reflected by the boundary, corresponding to a tangential discontinuity. This boundary condition in the 2-D simulation will lead to a large magnetic flux pileup at the magnetopause for $B_{y0} \neq 0$. The bow shock continuously propagates toward the front side, and thus the bow shock does not have a steady standoff distance in relation to the magnetopause. A second choice may be to allow a portion of the magnetic flux to be transported out through the boundary by $\mathbf{E} \times \mathbf{B}$ drift, where $\mathbf{E}$ is the electric field

and can be adjusted at the boundary. In the present simulation, we show only the results without the removal of magnetic flux. The tangential electric field is set to be zero at the magnetopause.

We assume that across the initial RD the physical quantities experience a jump only along the discontinuity normal, which is the propagation direction of RD. The quantities are uniform in other directions, and the discontinuity front is planar. This rotational discontinuity is thus locally a 1-D structure, while its propagation direction can have an arbitrary angle with the bow shock. In a plasma with an isotropic temperature the direction of the tangential magnetic field can change arbitrarily across the rotational discontinuity, while the magnetic field strength and plasma density and pressure remain unchanged. The normal component of inflow velocity v_n at the rotational discontinuity satisfies

$$v_n = \pm B_n/\sqrt{\mu_0 \rho} \tag{1}$$

where ρ is the plasma density and the positive (negative) sign is applied if the normal incident velocity is parallel (antiparallel) to the normal component of magnetic field B_n. The change of the tangential velocity across the rotational discontinuity should obey the Walen relation,

$$\Delta \mathbf{V}_t = \pm \Delta \mathbf{B}_t/\sqrt{\mu_0 \rho} \tag{2}$$

where $\Delta \mathbf{V}_t$ is the variation of tangential flow velocity across RD and $\Delta \mathbf{B}_t$ is the change of tangential magnetic field. The normal component of magnetic field

$$B_n = \text{const} \tag{3}$$

at the rotational discontinuity. In our 2-D simulation, RD is assumed to propagate toward the bow shock along a given direction $\mathbf{k}$, which is also the normal direction of RD. The propagation speed of RD in relation to the solar wind is determined from (1). When RD propagates to various positions, the magnetic field at the corresponding positions at the frontside semicircular boundary changes direction, and the flow velocity changes according to (2). The width of the initial RD is assumed to be about $3\lambda_0$.

In the calculation the ions are accelerated by electromagnetic forces. The electric field is determined from the electron momentum equation, and it is then used in Faraday's law to advance the magnetic field. The code utilizes the subcycling of the advance of the magnetic field to the advance of the particle. In our simulation the magnetic field is advanced 10 time steps for every time step the particles are advanced.

In addition to the 2-D simulation, for comparison we also show the results of 1-D simulations, which solve the Riemann problem associated with the BS/RD interaction. In the 1-D system, all the dependent variables are functions of the spatial coordinate x and time t only, while the normal direction of BS and RD is assumed to be in the x direction. Note that the x direction is also the normal of all the resulting discontinuities after the interaction, and the fronts of BS, RD, and resulting downstream discontinuities are planar, in the yz plane. In this system the normal component of the magnetic field $B_n = B_x$ is a constant, because $\nabla \cdot \mathbf{B} = 0$ and Faraday's law must be satisfied. Compared to the 2-D simulation, the 1-D simulation has the advantage of running a much longer system, over $500\lambda_0$ in our simulation, while using much fewer particles. Because of its high resolution the structure of the resulting discontinuities and pressure pulses is seen more clearly. A comparison between the 1-D hybrid simulation results and the 1-D ideal MHD theory of BS/RD interaction has been given by *Lin et al.* [1996]. In the 1-D simulation, initially at $t = 0$, the ratios of downstream to upstream quantities at the bow shock are determined by the MHD Rankine-Hugoniot jump relations of a fast shock, and the rotational discontinuity RD propagates toward the bow shock from upstream along the $-\mathbf{x}$ direction.

The 1-D hybrid code used in our study is that described by *Swift and Lee* [1983]. In our simulation the length per cell is $0.158\lambda_0$. The simulation domain length is $L_x = 4000$ grids. Two buffer zones are located at the two ends of the simulation domain. The ion number density upstream of the bow shock is $N_0 = 25$-50. The bow shock and initial rotational discontinuity have a half width of 2-$4\lambda_0$. The initial position of the bow shock is at $x_F = 0.6L_x$, and that of the rotational discontinuity is at $x_R = 0.8L_x$.

In the next two sections we present simulation results for four cases. In section 3, two cases with $B_{y0} = 0$ are first shown. The bow shock with a steady standoff distance in relation to the magnetopause is formed in these cases. The other two cases with $B_{y0} \neq 0$ are studied in section 4. The normalization of physical quantities is as follows. The magnetic field B is normalized to B_0, the ion number density N is normalized to N_0, the flow velocity V is normalized to V_{A0}, and the time t is normalized to Ω_0^{-1}. The thermal and magnetic pressures are expressed in units of $P_0 \equiv B_0^2/\mu_0$, which is equal to $N_0 V_{A0}^2$.

3. Simulation Results for Cases With $\mathbf{B_{y0} = 0}$

In case 1 the IMF $B_{x0} = -0.45B_0$, $B_{z0} = 0.9B_0$, and $B_{y0} = 0$. The solar wind speed is $V_0 = 5V_{A0}$ along the $-x$ direction, which corresponds to an Alfven Mach number $M_A = V_0/V_{A0} = 5$. An interplanetary rotational discontinuity propagates to BS along the direction $\mathbf{k} = -\mathbf{x}$. Across RD its tangential magnetic field rotates by $\Delta\Phi = 120^o$.

We first show the 1-D hybrid simulation results for case 1, which approximate the results along the Sun-Earth line, where the normal direction of both BS and RD is in the x direction. The shock normal angle of BS is $\theta_{Bn} \equiv \tan^{-1}(B_t/B_n) = 63.4^o$, where B_t is the tangential magnetic field. Figure 2 shows the hodogram of tangential magnetic field and spatial profiles of B_y, B_z, B^2, ion number density N, thermal pressure perpendicular to the magnetic field $P_\perp$ (solid line), parallel pressure $P_\parallel$ (dotted line), perpendicular temper-

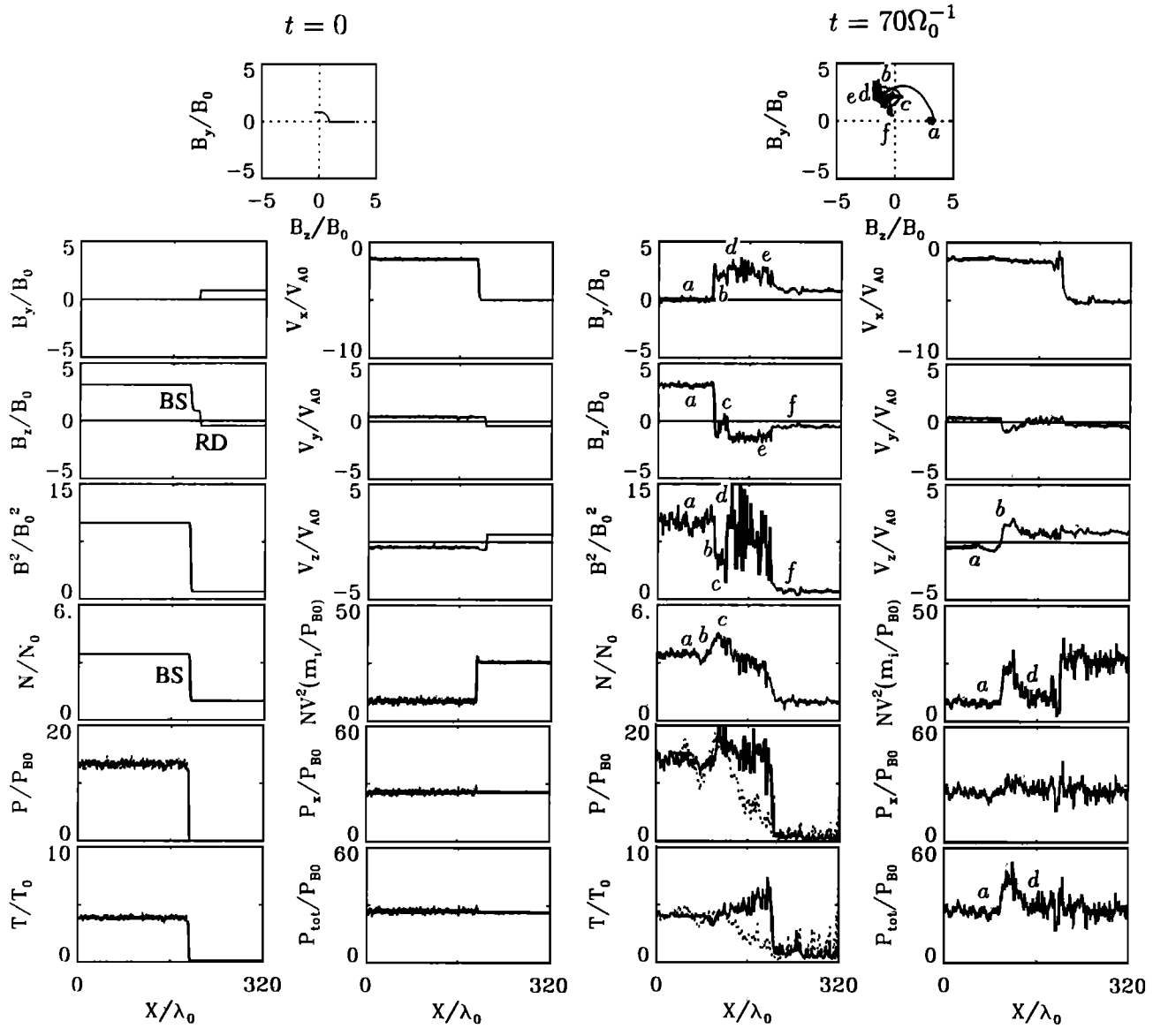

Figure 2. The 1-D simulation results of case 1: hodogram of tangential magnetic field and spatial profiles of B_y, B_z, B^2, ion number density N, thermal pressures (solid for $P_\perp$ and dotted for $P_\parallel$), temperatures (solid for $T_\perp$ and dotted for $T_\parallel$), V_x, V_y, V_z, dynamic pressure m_iNV^2, total pressure $P_{tot} \equiv (P + B^2/2\mu_0 + Nm_iV^2)$, and total pressure $P_x \equiv (P + B^2/2\mu_0 + Nm_iV_x^2)$ associated with the normal flow velocity at $t = 0$ and $t = 70\Omega_0^{-1}$. The pressure terms are normalized to $P_{B0} \equiv B_0^2/\mu_0$. At $t = 0$ an interplanetary rotational discontinuity (RD) is located upstream of the bow shock (BS). At $t = 70\Omega_0^{-1}$ a pressure pulse is present downstream of BS from *a* to *d*.

ature $T_\perp$ (solid line), parallel temperature $T_\parallel$ (dotted line), V_x, V_y, V_z, dynamic pressure m_iNV^2, total pressure $P_{tot} \equiv (P + B^2/2\mu_0 + Nm_iV^2)$, and total pressure $P_x \equiv (P + B^2/2\mu_0 + Nm_iV_x^2)$ associated with the normal flow velocity at $t = 0$ and $t = 70\Omega_0^{-1}$, where m_i is the ion mass. Here, $P = (P_\parallel + 2P_\perp)/3$. Note that the pressure terms in the figure are normalized to $P_{B0} = B^2/\mu_0$, and the tangential flow velocity shown in Figure 2 is calculated in the frame in which the initial dynamic pressure is a constant across the initial RD. The initial bow shock is located at $x = 175\lambda_0$, and the rotational discontinuity is at $x = 205\lambda_0$. The reason for plotting P_{tot} in addition to P_x is that in general, especially at the flanks, the flow tangential to the bow shock front may have a normal component at the magnetopause that contributes to the dynamic pressure at the magnetopause and causes it to move inward and outward.

The initial rotational discontinuity reaches the bow shock at $t \simeq 8\Omega_0^{-1}$. At $t = 70\Omega_0^{-1}$ after the BS/RD interaction a rotational discontinuity RD1, with a large magnetic field rotation from *a* to *b*, propagates in the downstream region of the bow shock, as shown in the field profiles and hodogram. The field rotation angle across RD1 is almost the same as the initial angle $\Delta\Phi$. Because of the presence of the temperature anisotropy

the magnetic field (plasma density) decreases (increases) across RD1. The bow shock is located between an upstream point f and a downstream point e, across which the magnetic field and plasma density increases while the flow speed decreases. Two slow shocks, SS1 from b to c and SS2 from d to c, propagate behind RD1 [see also *Lin et al.*, 1996]. Across the slow shock the magnetic field decreases, and plasma density increases.

To understand the results shown in Figure 2, we briefly introduce the MHD theory of the shock/shock interaction. According to ideal MHD theory, once the initial RD reaches the bow shock, it cannot simply penetrate through the bow shock without generating other discontinuities. This feature is due to the change in the Alfven speed across the bow shock, which is caused by the changes in the magnetic field and plasma density. Slow shocks must be generated to match the plasma flow velocity from the initial unperturbed downstream region of BS to the new upstream condition (see *Yan and Lee* [1996] for a detailed discussion). A plasma density plateau is thus formed downstream of the bow shock after the BS/RD interaction. The field rotation angle of the initial RD will also be modified in the downstream region of the bow shock. Our study based on the ideal MHD theory shows that in general, located from the Earth side, a weak fast expansion wave FE, a rotational discontinuity RD1, a slow shock SS1, a contact discontinuity CD, a slow shock SS2, a weak rotational discontinuity RD2, and a fast shock BS' are generated after the BS/RD interaction [*Lin et al.*, 1996].

The strength and position of the fast shock BS' are almost the same as those of the initial bow shock BS. The normal component of the flow velocity is superfast upstream of the fast shock and subfast and superintermediate downstream [e.g., *Landau and Lifshitz*, 1960]. The discontinuities RD1 and SS1 propagate toward the magnetopause in the downstream plasma with the intermediate mode and slow mode speeds, respectively. Furthermore, the convection of downstream plasma allows RD1 and SS1 to move with a larger speed to the magnetopause. The speeds of RD1 and SS1 are very similar, and thus these two discontinuities are not separated. Similar results are found for RD2 and SS2. They propagate toward the Sun in the frame of the downstream plasma but are convected to the magnetopause, since the normal flow speed of the downstream plasma is much larger than the wave mode speeds of RD2 and SS2. The contact discontinuity simply convects with the flow.

In the hybrid simulation, however, the contact discontinuity CD cannot be identified because of the mixing of ions from both sides along the magnetic field [*Lin and Lee*, 1993], and the small rotational discontinuity RD2 and fast expansion wave FE are too weak to be clearly seen.

An ion density enhancement of 30% is found across RD1 and SS1, as seen in the hybrid simulation results in Figure 2. The magnetic field decreases in the region of the density enhancement. This structure has been interpreted as a slow mode structure in the magnetosheath [*Yan and Lee*, 1994]. A temperature anisotropy is present in the downstream discontinuities, and the temperature is nearly constant. In the region of the density enhancement the normal flow velocity remains almost constant, and the total pressure P_x associated with V_x increases about 25% of the background value. On the other hand, a large variation in the tangential flow velocity is present from a to d, as is seen in the V_z profile of Figure 2. The variations in the tangential flow speed and plasma density lead to a large dynamic pressure pulse downstream of the bow shock, as is shown in the NV^2 profile. Correspondingly, the total pressure P_{tot} increases by nearly 100% of the background value in the magnetosheath. At rotational discontinuities or slow shocks the sum of the thermal and magnetic pressure $(P + B^2/2\mu_0)$ remains nearly constant. The increase in the dynamic pressure $m_i NV^2$, however, leads to an increase in the total pressure. It is found that the pressure pulse propagates to the magnetopause with nearly constant amplitude. The time duration of the propagating pressure pulse is estimated to be ~1 min, and the time for the pressure pulse to nearly reach the magnetopause from the bow shock is ~2-3 min [*Lin et al.*, 1996].

Since RD1 and the slow shocks are not clearly separated in the simulation, the structure that consists of RD1, SS1, and SS2 will be termed RD1. It is characterized by a change in the magnetic field direction, a decrease in the field magnitude, and an increase in the plasma density.

Figure 3 illustrates the structure of magnetic field and flow velocity in case 1 before and after the BS/RD interaction. Before the interaction, as shown on the left-hand side of Figure 3, RD propagates to BS along the $-x$ direction. The fronts of RD and BS divide the system into three regions, with region 1 being the downstream region of RD, region 2 being in the upstream of both BS and RD, and region 3 being the downstream region of BS. The magnetic field **B** increases in the z direction across BS, while it changes direction across RD. The flow velocity **V**, as shown by bold arrows, de-

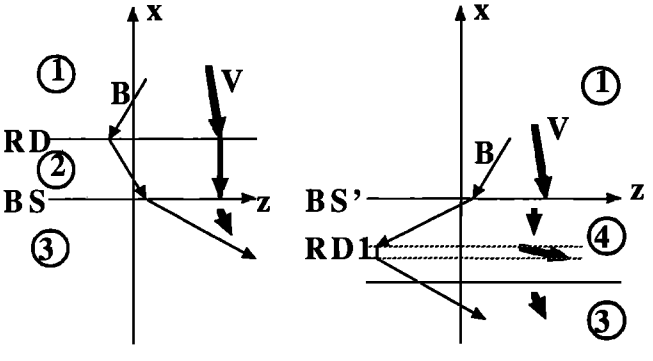

Figure 3. Schematic plot for the structure of magnetic field **B** and flow velocity **V** (bold arrows) in case 1. (left) Before the BS/RD interaction the fronts of RD and BS divide the system into three regions, regions 1 through 3. RD propagates to BS along $-x$. (right) After the interaction a dynamic pressure pulse is formed at RD1 between dotted lines in region 4 downstream of the new bow shock BS'.

creases across BS from upstream to downstream, while it changes slightly across RD in the upstream of the high Mach number bow shock. Note that the changes in B_z and V_z across RD are in the opposite direction in this case, according to the Walen relation (2). After the interaction between BS and RD the magnetic field increases in the $-z$ and $+y$ (not shown) directions across the new bow shock BS', and the flow velocity decreases, as shown on the right-hand side of Figure 3. A large kink in the magnetic field appears in region 4, the downstream region of BS', between the unperturbed fields in regions 1 and 3. The structure RD1 is present in this kink field region between the dotted lines, and the tangential flow velocity is greatly enhanced in RD1 because of the field tension force. Meanwhile, the plasma density also increases in RD1, and the magnetic field decreases. A dynamic pressure pulse is formed at RD1.

On the basis of the 1-D model we have carried out a parameter search for the amplitude of the pressure pulse [*Lin et al.*, 1996]. The strength of the pressure pulse is found to increase with $|\Delta\Phi|$ across the incident RD, where $-180^o < \Delta\Phi < 180^o$, and increase with the shock normal angle θ_{Bn}. On the other hand, the strength decreases with the Alfven Mach number M_A and the upstream β_0. For typical solar wind conditions the strength of the pressure pulse can be up to 100%.

The 2-D hybrid simulation results of case 1 are given below. The left column of Figure 4 shows, from top to bottom, magnetic field vectors in the xy plane, plasma flow vectors in the xy plane, the contours of magnetic field B, ion number density N, flow speed V, and total pressures $P_{tot} = (P + m_i NV^2 + B^2/2\mu_0)$ at $t = 55\Omega_0^{-1}$. A bow shock has formed in front of the magnetopause, as indicated in Figure 4. Across the front of BS the magnetic field in the xy plane increases toward the two flank sides. Correspondingly, the plasma flow decreases and diverges to the two sides. The ion density increases. Also seen in Figure 4 is an incoming interplanetary rotational discontinuity RD. The magnetic field changes direction across RD, and the flow velocity also changes, as can be seen in Figure 4. This rotational discontinuity is incident into the simulation domain at $t = 40\Omega_0^{-1}$ from the upstream boundary. Note that when RD starts to flow into the domain, the BS has not reached a steady position. By the time RD reaches BS, the bow shock has evolved to a nearly steady position.

The right column of Figure 4 displays the simulation results at $t = 80\Omega_0^{-1}$. At this time the incident rotational discontinuity has passed the bow shock. Upstream of the bow shock the IMF has completely changed its orientation to be that in the downstream of the incident RD, with $B_x = B_{x0} = -0.45B_0$, $B_y = 0.866B_{z0} = 0.78B_0$, and $B_z = -0.5B_{z0} = -0.45B_0$. The bow shock stands at a steady distance of $\sim$18.5 R_E from the magnetopause along the Sun-Earth line. The position and strength of the new bow shock are nearly the same as those of the original BS in a quasi-steady state without the interaction. The magnetic field increases in this new direction across the bow shock, as shown in the field vector plot in Figure 4. A a result, kinked field lines are formed between the new and the unperturbed plasma regions in the magnetosheath. Associated with these kinked field lines, a region with an enhancement in plasma density and a decrease in magnetic field is generated. The flow speed experiences a change due to the field tension. This structure corresponds to RD1 obtained in the 1-D simulation. This perturbation in the field and plasma propagates toward the Earth and forms a curved front between the bow shock and the magnetopause, as shown in the field, plasma density, and flow velocity contour plots. Correspondingly, a pressure pulse exists in the region of the perturbation, as indicated in the contour plot of P_{tot}. As the pressure pulse approaches the magnetopause, it is slowed down, because the plasma convection speed and the wave speeds of intermediate and slow modes normal to the magnetopause decrease to zero. The simulation is not carried out for the further interaction of this pressure pulse with the magnetopause. Nevertheless, it is expected that the arrival of the pressure pulse will cause a wavy motion of the magnetopause.

Note that a slow mode-like structure is also present in front of the magnetopause while the initial bow shock is formed if the configurations of physical quantities at $t = 0$ are very different from those for the steady bow shock.

Figure 5 shows the spatial profiles of physical quantities along the r direction at $\theta = 90^o$, which is along the Sun-Earth line. Presented in the left column are the profiles of B_r, B_z, B_θ, field magnitude B, flow velocities V_r, V_z, and V_θ, total flow speed V, ion number density N, perpendicular temperature $T_\parallel$ (dotted lines), parallel temperature $T_\perp$ (solid lines), and total pressures P_{tot} (solid lines) and $P_r \equiv (P + B^2/2\mu_0 + m_i NV_r^2)$ (dotted lines) at $t = 55\Omega_0^{-1}$. The middle column shows the spatial profiles at $t = 68\Omega_0^{-1}$, and the results at $t = 80\Omega_0^{-1}$ are shown in the right column.

At $t = 55\Omega_0^{-1}$ the interplanetary rotational discontinuity RD is in the upstream region of the bow shock BS and is located at the position $r \simeq 23\ R_E$, as indicated in the left column of Figure 5. In the downstream region of RD, which is on the sunward (right) side, the components of the flow velocity change, while the flow speed is nearly unchanged. At this quasi-perpendicular shock BS the perpendicular temperature is much higher than the parallel temperature. The total pressure P_{tot} is nearly constant everywhere. At $t = 68\Omega_0^{-1}$, RD has interacted with the bow shock, and the structure RD1 with magnetic field changing direction appears just downstream of the bow shock, as indicated in the middle column of Figure 5. A pressure pulse appears correspondingly, but it is not clearly separated from the bow shock at this moment.

At $t = 80\Omega_0^{-1}$ the structure RD1 has propagated midway between the bow shock and the magnetopause, at $r \simeq 13.4\ R_E$. A large change in V_z and in the total flow speed V is present at this structure. Notice that in the 2-D simulation the slow shocks are hardly seen. This phenomenon may also be due to the large ion inertial length λ_0 and ion gyroradius used in the model, in addition to the fact that the propagation speeds of the

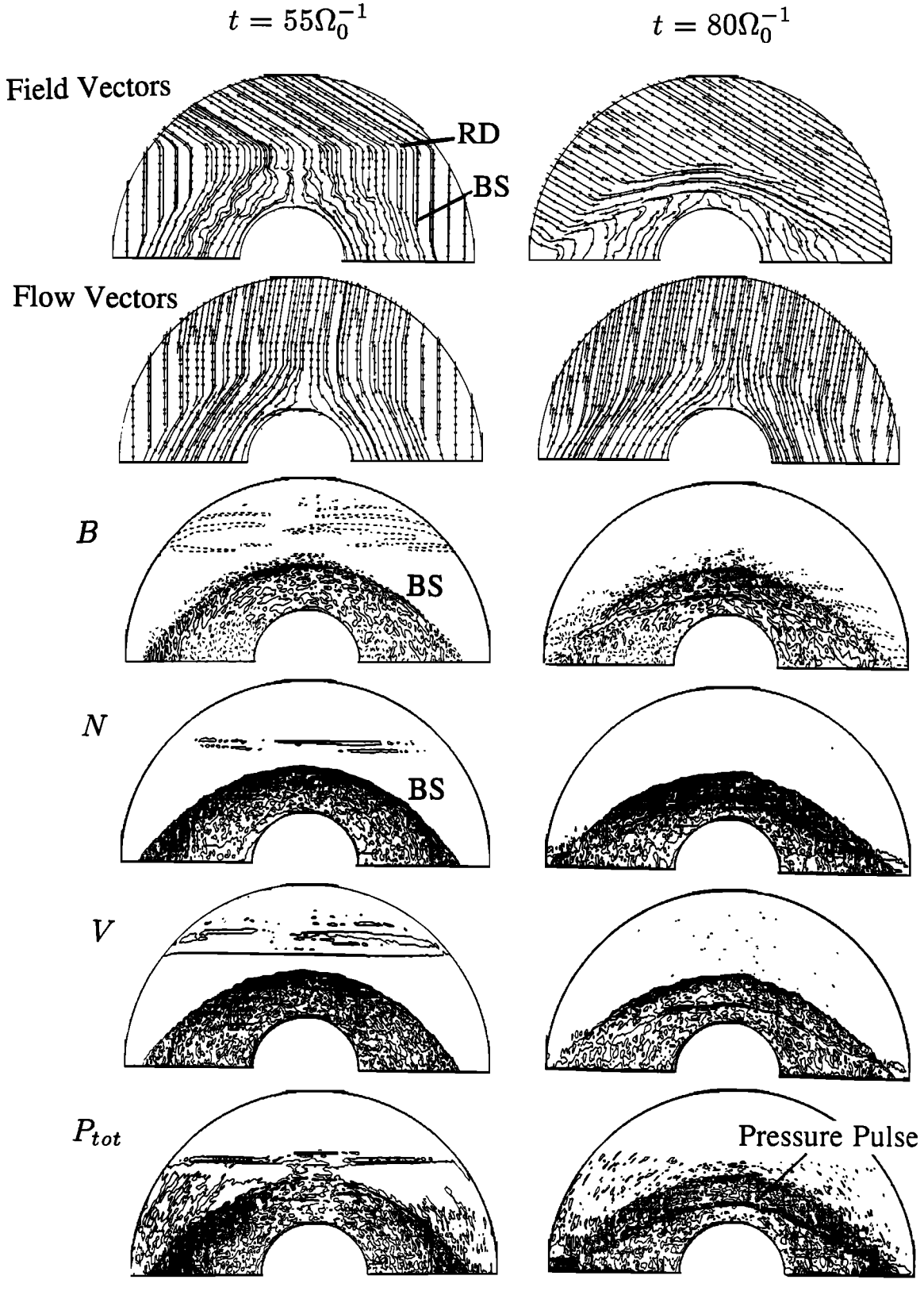

Figure 4. The 2-D simulation results of case 1. (left) From the top, magnetic field vectors in the xy plane, plasma flow vectors in the xy plane, contours of magnetic field B, ion number density N, flow speed V, and total pressures P_{tot} at $t = 55\Omega_0^{-1}$. The incoming rotational discontinuity RD is propagating toward the bow shock BS from upstream. (right) Results at $t = 80\Omega_0^{-1}$.

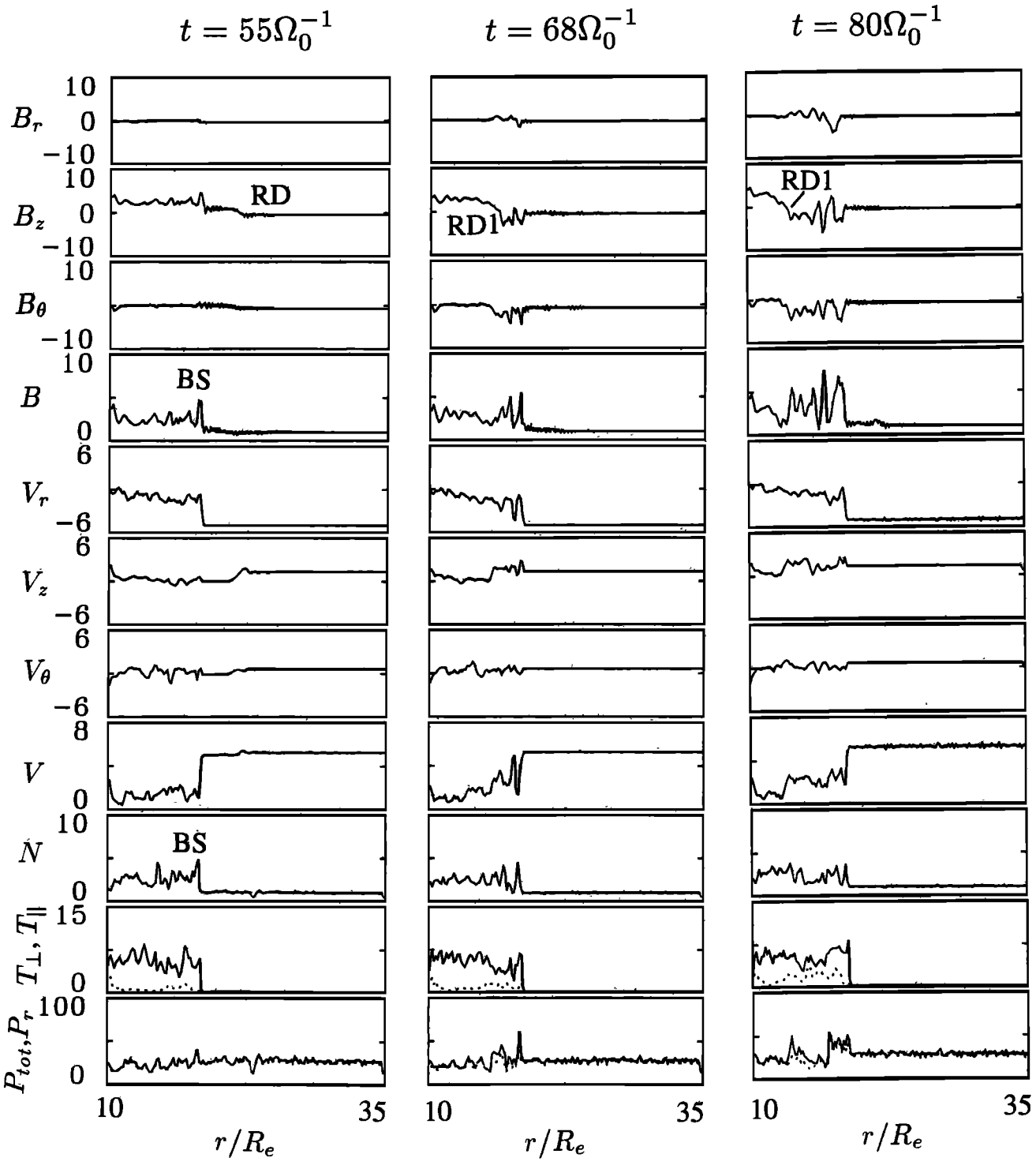

Figure 5. Spatial profiles of normalized quantities B_r, B_θ, B_z, field magnitude B, flow velocities V_r, V_θ, and V_z, total flow speed V, ion number density N, perpendicular temperature $T_\parallel$ (dotted lines), parallel temperature $T_\perp$ (solid lines), and total pressures P_{tot} (solid lines) and P_r (dotted lines) along the r direction at $\theta = 90°$, the Sun-Earth line. The distance r is in units of Earth radii. Here, (left) for $t = 55\Omega_0^{-1}$, (middle) $68\Omega_0^{-1}$, and (right) $80\Omega_0^{-1}$. A pressure pulse is present in the structure RD1, which is mainly a rotational discontinuity resulting from the BS/RD interaction.

rotational discontinuity and slow shocks are very close. A large pulse in the plasma dynamic pressure NV^2 (not shown) and thus in P_{tot} are present in this region. The total pressure P_{tot} increases by nearly 100%, as shown in Figure 5. The total pressure P_r associated with $m_i N V_r^2$ increases by about 20-30%.

For comparison, Figure 6 shows the spatial profiles of B_z, B_θ, N, V, P_{tot}, and P_r along $\theta = 45°$ and $135°$ at

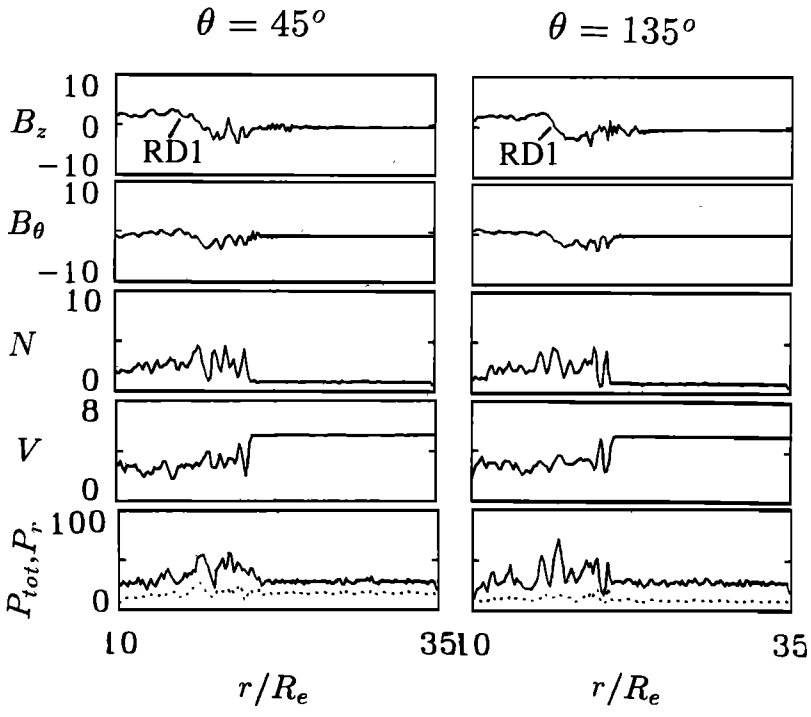

Figure 6. Spatial profiles of normalized physical quantities along $\theta = 45^o$ and 135^o at $t = 75\Omega_0^{-1}$ obtained from the 2-D simulation of case 1. The dotted lines are for P_r.

$t = 75\Omega_0^{-1}$, corresponding to two positions near dawn (left) and dusk (right) flanks, respectively. At $\theta = 45^o$, P_{tot} increases by about 80%. A strong pressure pulse in P_r is also present at RD1. In the flank region the total flow velocity in the magnetosheath is large in comparison with that in the subsolar region, and the change of flow speed at RD1 is not as significant. At the dawnside, across the new bow shock, the flow is decelerated to a speed larger than that in the original unperturbed magnetosheath. It then decreases to the unperturbed value across RD1. The jump of the flow velocity across RD1 is mainly in the tangential direction of the RD1 front. In comparison with the subsolar region a larger part of the r component velocity comes from the tangential velocity because of the flaring of the RD1 front. Therefore the pulse in P_r is stronger than that in the subsolar region.

On the other hand, at $\theta = 135^o$ the kink of field lines is to slightly accelerate the flow. As a result the change in V_r here is not as sharp as that at $\theta = 45^o$. The increase in P_r at the pressure pulse is only slightly.

In case 1 the bow shock is a quasi-perpendicular shock, and there is no apparent effect of reflected ions. We now present the 2-D simulation results of case 2, in which $B_{x0} = -0.96B_0$, $B_{y0} = 0$, and $B_{z0} = 0.26B_0$. The bow shock BS is a quasi-parallel shock in most regions except where θ is close to 0^o and 180^o. The interplanetary rotational discontinuity RD is incident into the simulation domain at $t = 70\Omega_0^{-1}$ with $\mathbf{k} \parallel -\mathbf{x}$ and $\Delta\Phi = 120^o$.

Unlike in case 1, disturbances are present in the upstream region of the bow shock. The distance between the bow shock and the magnetopause is much smaller in this case than in case 1. Reflected ions are found in the upstream region of BS. After the IMF changes its direction, the bow shock in the subsolar region and on the duskside (left side) is still a quasi-parallel shock. On the dawnside (right side) the bow shock has become a quasi-perpendicular shock, and the upstream appears quiet. While the IMF changes direction, the reflected ions are found to generate a fast wave and an associated pressure pulse, which interacts with the bow shock and produces a pressure pulse in the magnetosheath.

The spatial profiles of B_z, B_θ, B, N, V, P_{tot}, and P_r are shown in Figure 7 for $\theta = 60^o$ at $t = 102\Omega_0^{-1}$, $107\Omega_0^{-1}$, and $112\Omega_0^{-1}$. At $t = 102\Omega_0^{-1}$, RD1 appears in the magnetosheath, as indicated in Figure 7. The amplitude of RD1 is small because of the small θ_{Bn} in this case. Correspondingly, there is no significant increase in P_{tot} associated with RD1 in the magnetosheath, as obtained from the 1-D model. On the other hand, a fast wave (FW) is present upstream of the bow shock, as indicated in Figure 7. The magnetic field, plasma density, dynamic pressure $m_i NV^2$ (not shown), and P_{tot} are positively correlated at FW. This wave is generated by the interaction between the incident discontinuity RD and the reflected ions from the quasi-parallel BS. It originally propagates sunward in the upstream plasma but is carried by the upstream solar wind toward the bow shock when the local quasi-parallel shock becomes a quasi-perpendicular shock. Notice that the solar wind bulk inflow is slowed near the bow shock because of the ion reflection. The upstream pressure structure has a spatial length of roughly 15 R_E in the simulation. Considering that the simulation parameters have been rescaled to make the calculation run more cost effec-

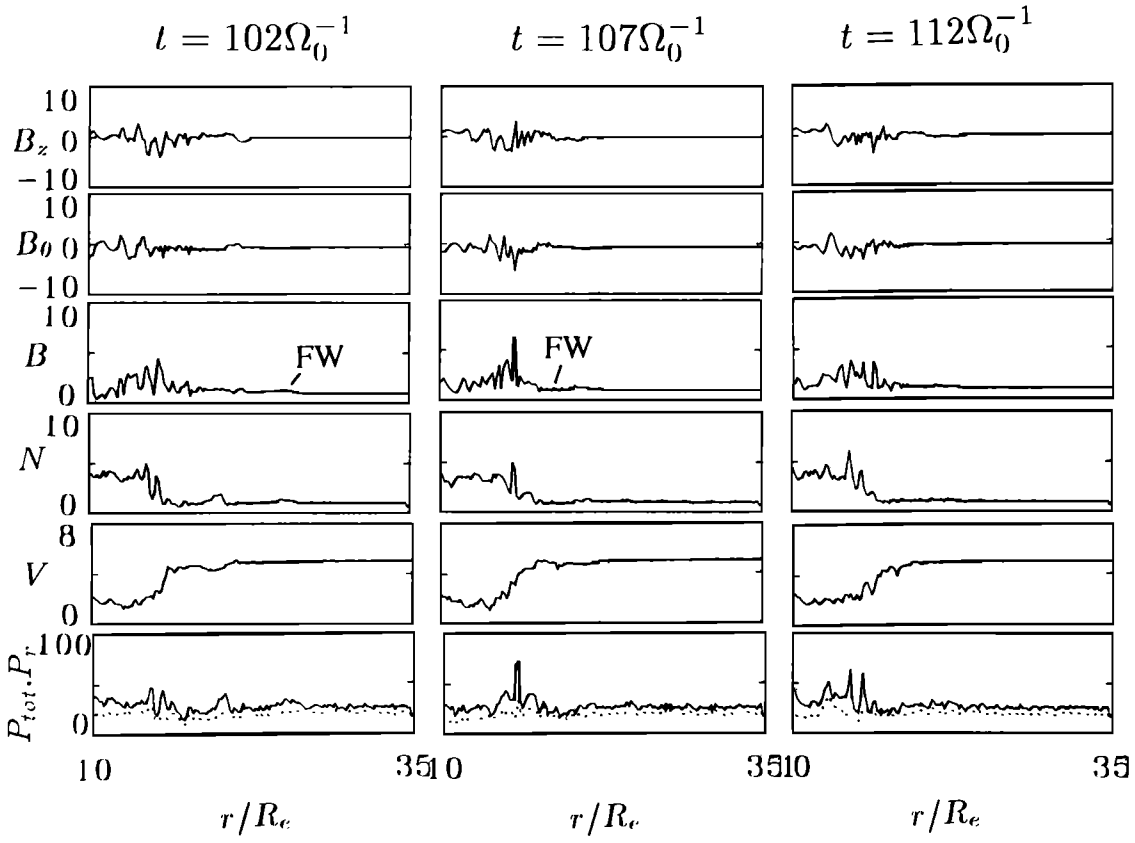

Figure 7. Simulation results of case 2: spatial profiles of physical quantities for $\theta = 60^o$ at (left) $t = 102\Omega_0^{-1}$, (middle) $t = 107\Omega_0^{-1}$, and (right) $t = 112\Omega_0^{-1}$. The dotted lines are for P_r. A pressure pulse associated with the fast wave FW is present upstream of the bow shock in the BS/RD interaction.

tively, the spatial length of the upstream wave may be of the order of a few earth radii. It may correspond to a time duration of a few minutes, as discussed by *Sibeck et al.* [1989] and *Fairfield et al.* [1990].

At $t = 107\Omega_0^{-1}$ the fast wave reaches the bow shock, and a peak in magnetic field, plasma density, perpendicular temperature (not shown), and total pressure is found right at the bow shock. At $t = 112\Omega_0^{-1}$ the total pressure P_{tot} increases downstream of the bow shock, and a 100% increase in P_r is present. This downstream pressure pulse propagates in the magnetosheath plasma to the magnetopause with the fast mode speed. Eventually in the simulation, it hits the magnetopause boundary.

In the 2-D simulation it is found that when a local quasi-parallel bow shock changes to a quasi-perpendicular shock because of the change in the IMF direction, a pressure pulse associated with a fast wave may be present in the foreshock region of the bow shock, because the reflected ions at the bow shock cannot escape upstream of the quasi-perpendicular shock. All these ions in a relatively long range are carried back to the bow shock and produce an upstream pulse with an amplitude much greater than the background disturbances. The spatial length of the upstream pressure pulse is longer than that of upstream pulses generated locally at a quasi-parallel shock [e.g., *Thomas et al.*, 1995].

4. Simulation Results for Cases With $B_{y0} \neq 0$

Next we present the results for general cases in which the magnetic field has the component $B_{y0} \neq 0$. In case 3 the initial IMF is in the xy plane, with $B_{x0} = -0.707B_0$, $B_{y0} = -0.707B_0$, and $B_{z0} = 0$. It makes an angle of 45^o with $-x$ and $-y$ directions. The solar wind inflow velocity is assumed to be 5 times V_{A0}, along the $-x$ direction. An interplanetary rotational discontinuity is assumed to propagate into the simulation domain at $t = 30\Omega_0^{-1}$ along the $-x$ direction. The tangential magnetic field rotates an angle $\Delta\Phi = 120^o$ across RD.

Figure 8 shows the field vectors and flow vectors in the xy plane and the contours of magnetic field, ion density, flow speed, and total pressure P_{tot} at $t = 40\Omega_0^{-1}$ (left column), $62\Omega_0^{-1}$ (middle column), and $70\Omega_0^{-1}$ (right column). At $t = 40\Omega_0^{-1}$ the bow shock is developing and propagating toward the Sun. On the dawnside the bow shock is a quasi-parallel shock, with the upstream magnetic field nearly perpendicular to the shock front. The magnetic field exhibits disturbances in the upstream, as seen from the field vector plot and the contour plots of the field and flow velocity. On the duskside the bow shock is a quasi-perpendicular shock, and the upstream appears to be quiet. Note that the shock front of BS is asymmetric about the x axis. The incoming RD has

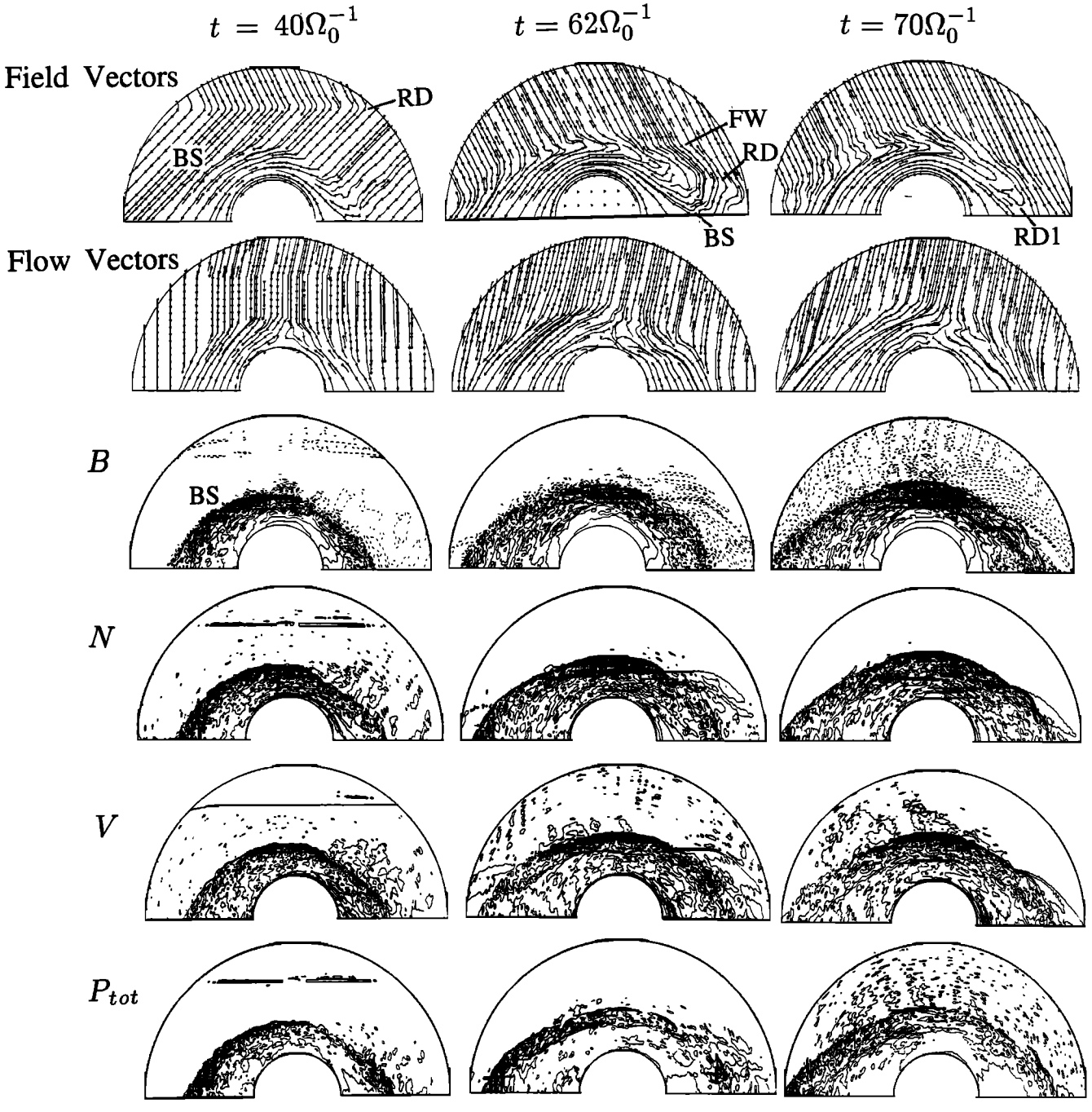

Figure 8. Results of case 3: magnetic field vectors and flow vectors in the xy plane and contours of magnetic field, ion density, flow speed, and total pressure at (left) $t = 40\Omega_0^{-1}$, (middle) $62\Omega_0^{-1}$, and (right) $70\Omega_0^{-1}$. FW indicates the front of the fast wave generated by the variation of the IMF orientation.

reached a certain distance from the upstream boundary, across which the IMF changes its direction.

At $t = 62\Omega_0^{-1}$ the rotational discontinuity has just passed BS in the subsolar region and on the dusk-side flank. Kinked magnetic field lines appear in the downstream region. In the dawnside flank region with $\theta < 45^o$, however, the propagation speed of RD is slowed down because of the reduced plasma inflow speed at the quasi-parallel BS. The incident rotational discontinuity has not reached BS. A new FW front develops upstream of the original BS, as indicated in Figure 8. The magnetic field in the xy plane is bent toward the dawn through the front of FW, and the incoming RD is located between this wave front and the original BS, as shown in the field vector plot in the middle column of Figure 8. FW propagates in the upstream direction in the plasma but is carried by the solar wind flow toward BS. The magnetic field and plasma are fairly active up-

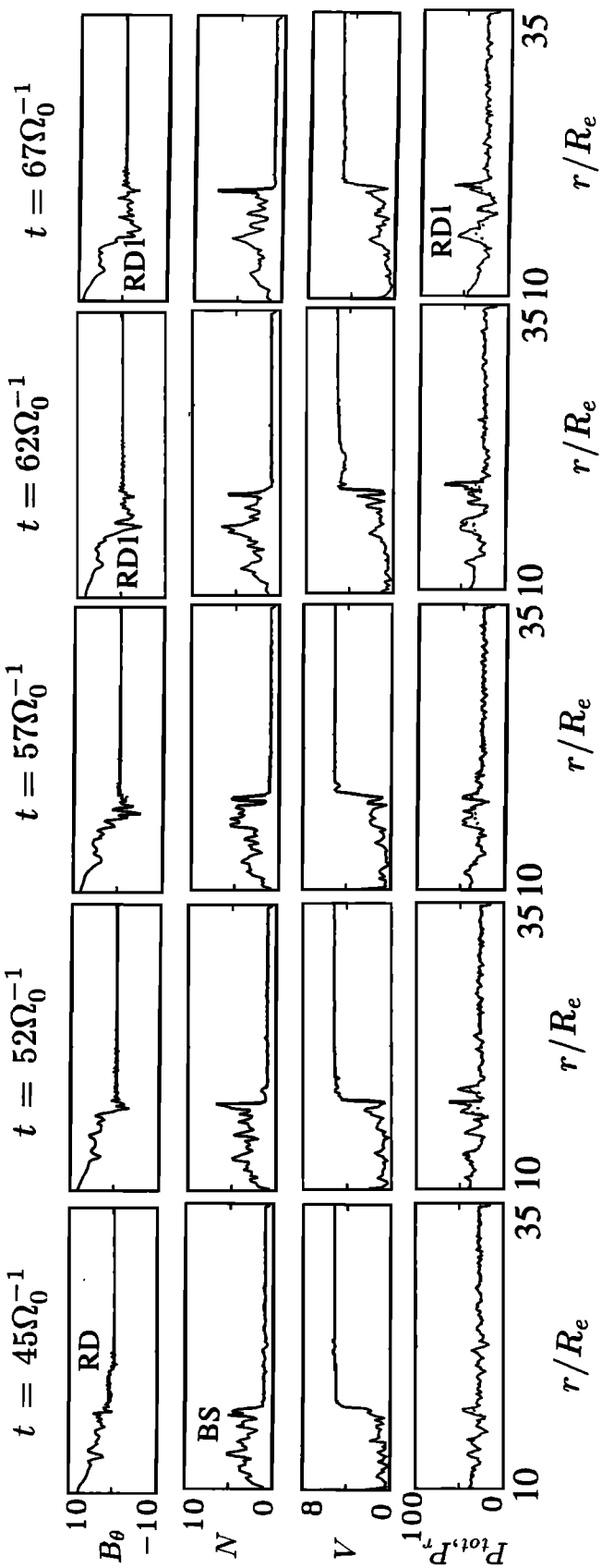

Figure 9. Spatial profiles of physical quantities for case 3 along $\theta = 90^o$ in a time series from $t = 45\Omega_0^{-1}$ to $67\Omega_0^{-1}$.

stream of BS, as can be seen from the field and plasma contours. The appearance of FW is also seen in other regions with $\theta < 90^o$ at earlier times.

At $t = 70\Omega_0^{-1}$, FW has nearly propagated through the bow shock at all the local times. Now the bow shock on the dawnside becomes a quasi-perpendicular shock. On the duskside the bow shock has changed from a quasi-perpendicular to a quasi-parallel shock, and the upstream appears to be more active than it was at $t = 40\Omega_0^{-1}$. Again the bow shock front is asymmetric about the x axis. The kinked field lines associated with RD1 are seen in the downstream. A front of pressure pulse is found in the magnetosheath. Since the magnetic flux cannot pass around the magnetopause in the 2-D simulation, the bow shock continuously expands to upstream, and the distance between the bow shock and the pressure pulse increases with time.

Figure 9 presents the spatial profiles of B_θ, N, V, P_{tot}, and P_r for case 3 along $\theta = 90^o$ in a time series with $t = 45\Omega_0^{-1}$, $52\Omega_0^{-1}$, $57\Omega_0^{-1}$, $62\Omega_0^{-1}$, and $67\Omega_0^{-1}$. At $t = 45\Omega_0^{-1}$, RD is in the upstream and near BS, as indicated in Figure 9. It arrives at BS at $t = 52\Omega_0^{-1}$. At $t = 57\Omega_0^{-1}$, RD1 starts to appear in the downstream. It is seen to be separated from the bow shock at $t = 62\Omega_0^{-1}$, as shown in the B_θ profile. A pressure pulse is generated in the magnetosheath, as shown in the P_{tot} and P_r profiles. At $t = 67\Omega_0^{-1}$, RD1 is farther away from the bow shock. The amplitude of the pressure pulse is about 100% of the background magnetosheath value in P_{tot} and about 40% in P_r. Notice that there is a pressure enhancement right at the bow shock at $t = 67\Omega_0^{-1}$. This is due to some transient process as the shock reverts to a more steady condition. The bow shock is still evolving and propagating in the simulation. It is found that eventually such enhancement tends to die out in time.

To examine the effects of reflected ions, we show in Figure 10 the spatial profiles of B_θ, B, N, V, $T_\perp$, $T_\parallel$, P_{tot}, and P_r for case 3 along $\theta = 45^o$, where the original BS is nearly a parallel shock. Shown in the figure is the evolution of the profiles through $t = 57$, 60, 63, and $67\Omega_0^{-1}$. At $t = 57\Omega_0^{-1}$, RD has just interacted with BS, and RD1 starts to develop, as shown in Figure 10. The shock front of the quasi-parallel shock is found to be poorly defined. In the upstream region of the bow shock a fast mode FW is present, in which the changes in magnetic field, ion density, and total pressure are in phase. This fast wave is carried by the solar wind and moves toward the bow shock. At $t = 60\Omega_0^{-1}$ while FW has not reached the bow shock, a pressure pulse is generated at RD1 in the magnetosheath. At $t = 63\Omega_0^{-1}$, the fast wave has an interaction with the bow shock, and another pressure pulse starts to form. This pressure pulse has passed the bow shock at $t = 67\Omega_0^{-1}$, and its amplitude in P_{tot} is about 100% of the background magnetosheath value. Note that the distance between RD1

and the bow shock increases with time, although there seems no apparent change in the distance between RD1 and the magnetopause. In the simulation the second pressure pulse, which is due to the reflected ions, eventually catches up the first pulse associated with RD1. The pressure P_r also seems to increase as correlated with P_{tot}.

In early times before RD reaches BS (not shown in Figure 10) the parallel temperature is nearly 3 times higher than the perpendicular temperature upstream of BS at $\theta = 45^o$, indicating the existence of reflected ions at the bow shock. As the IMF changes its direction, the ratio $T_\parallel/T_\perp$ decreases. At $t = 67\Omega_0^{-1}$ the bow shock has become a quasi-perpendicular shock, and $T_\perp$ is greater than $T_\parallel$. This bow shock has a well-defined shock front.

Figure 11 displays the spatial profiles of B_θ, V, P_{tot}, P_r, $T_\perp$, and $T_\parallel$ at various local times obtained from case 3 when the pressure pulse has just propagated to the middle between the bow shock and the magnetopause, so that the pressure pulse is not influenced by the boundary condition at the magnetopause. Plotted are the profiles from $\theta = 30^o$ to 150^o for every 15^o. The pressure pulses in the P_{tot} profiles at $\theta = 30^o$, 45^o, and 60^o have a strength of ~50-100%, and they are not as strong as those at the dusk side flank. The total pressure P_r associated with NV_r^2 also increases by ~30-50%. These pressure pulses are mainly due to the reflected ions being carried back by the changing of the IMF direction. The plasma flow is greatly decelerated by the field tension at the dawnside flank, and thus the pressure pulse associated with RD1 is not significant. On the other hand, the duskside pressure pulses at $\theta = 120^o$, 135^o, and 150^o are relatively strong, with an amplitude of ~200-300% in P_{tot}. This strength is due to the large acceleration in the flow speed V by the field tension force at RD1, as seen from the V profile. The pulse in P_r, however, appears to increase by only 10-40%, because V_r does not have a sharp change across RD1, similar to case 1. In the subsolar region with $\theta = 75^o$, 90^o, and 105^o the increase of P_{tot} at RD1 is about 100-150%, and the strength in P_r is about 50%.

A large parallel temperature $T_\parallel$ is found in the upstream of quasi-parallel shocks, as shown in Figure 11 for $\theta > 75^o$. In the dawnside profiles for $\theta < 75^o$, $T_\parallel$ becomes small.

Finally, we show case 4, in which RD propagates to BS with an oblique angle. In this case the initial IMF is along the $-y$ direction, with $B_{x0} = 0$, $B_{y0} = -B_0$, and $B_{z0} = 0$. The solar wind flow velocity $V_0 = 5V_{A0}$, along the $-x$ direction. At $t = 40\Omega_0^{-1}$, RD is incident into the simulation domain from the frontside boundary along the direction $\mathbf{k} = (-0.97, -0.26, 0)$, which makes an angle of 15^o with the $-x$ direction. The rotation angle of the tangential magnetic field of RD is $\Delta\Phi = 160^o$.

The top panel of Figure 12 shows the magnetic field vectors at $t = 55\Omega_0^{-1}$, and the second to sixth panels show, respectively, the field vectors, the flow vectors, and the contours of B, V, and P_{tot} at $t = 75\Omega_0^{-1}$. At $t = 55\Omega_0^{-1}$, RD is located in the upstream region of BS and propagating toward BS, as shown in Figure 12. The bow shock front is symmetric about the x axis. The interplanetary rotational discontinuity reaches and interacts with BS at $t = 60\Omega_0^{-1}$. At $t = 75\Omega_0^{-1}$, RD1 is present in the downstream region of the bow shock with $\theta < 150^o$, as shown in Figure 12. The upstream IMF has changed direction, and the bow shock front becomes slightly asymmetric. The front of RD1 is also asymmetric about the x axis, with the dawnside part closer to the magnetopause, consistent with the alignment of the front of initial RD. On the duskside the initial discontinuity RD has not completely passed through the bow shock at $t = 75\Omega_0^{-1}$.

A pressure pulse is found to be generated at RD1. The strength of this pressure pulse is about 50-100% in P_{tot} and 20-100% in P_r.

5. Summary

Two-dimensional hybrid simulations have been carried out to study the interaction between the bow shock and an interplanetary rotational discontinuity. In this study a curvilinear coordinate system is used in the simulation. Pressure pulses are found to be generated in the upstream and downstream of the bow shock as a result of the BS/RD interaction. The downstream pressure pulse propagates directly to the magnetopause. When a local quasi-parallel shock becomes a quasi-perpendicular shock because of the IMF changing direction, the upstream pressure pulses are present, carried by the solar wind to propagate through the bow shock, and also generate a pressure pulse to the magnetopause. The 2-D simulation is compared with 1-D simulations for the BS/RD interaction. The simulation results are summarized as follows.

1. In the 1-D hybrid simulation a structure RD1, consisting of a rotational discontinuity and two slow shocks, is generated in the downstream region of the bow shock. The bow shock strength and location after the interaction are almost the same as those initially, and the rotation angle of the tangential magnetic field across the downstream rotational discontinuity is nearly the same as that across the initial RD. A density enhancement and a magnetic field decrease are found throughout these downstream discontinuities, which propagate to the magnetopause. Across RD1 the tangential flow velocity has a significant change. A large dynamic pressure pulse in the m_iNV^2 profile is found in this region. Correspondingly, a pulse in the total pressure $P_{tot} = (P + B^2/2\mu_0 + m_iNV^2)$ is present. The pressure pulse propagates with RD1 to the magnetopause with a nearly constant amplitude. The time duration of the downstream pressure pulse is estimated to be ~1 min, and the time for the pressure pulse to nearly reach the magnetopause from the bow shock is ~2-3 min. The amplitude of the pressure pulse increases with the rotation angle $\Delta\Phi$ across the initial RD and the shock normal angle θ_{Bn} at the bow shock but decreases with the Alfven Mach number M_A and upstream plasma beta β_0 of the bow shock.

2. In the 2-D simulation a pressure pulse associated with RD1 is present in the magnetosheath after the

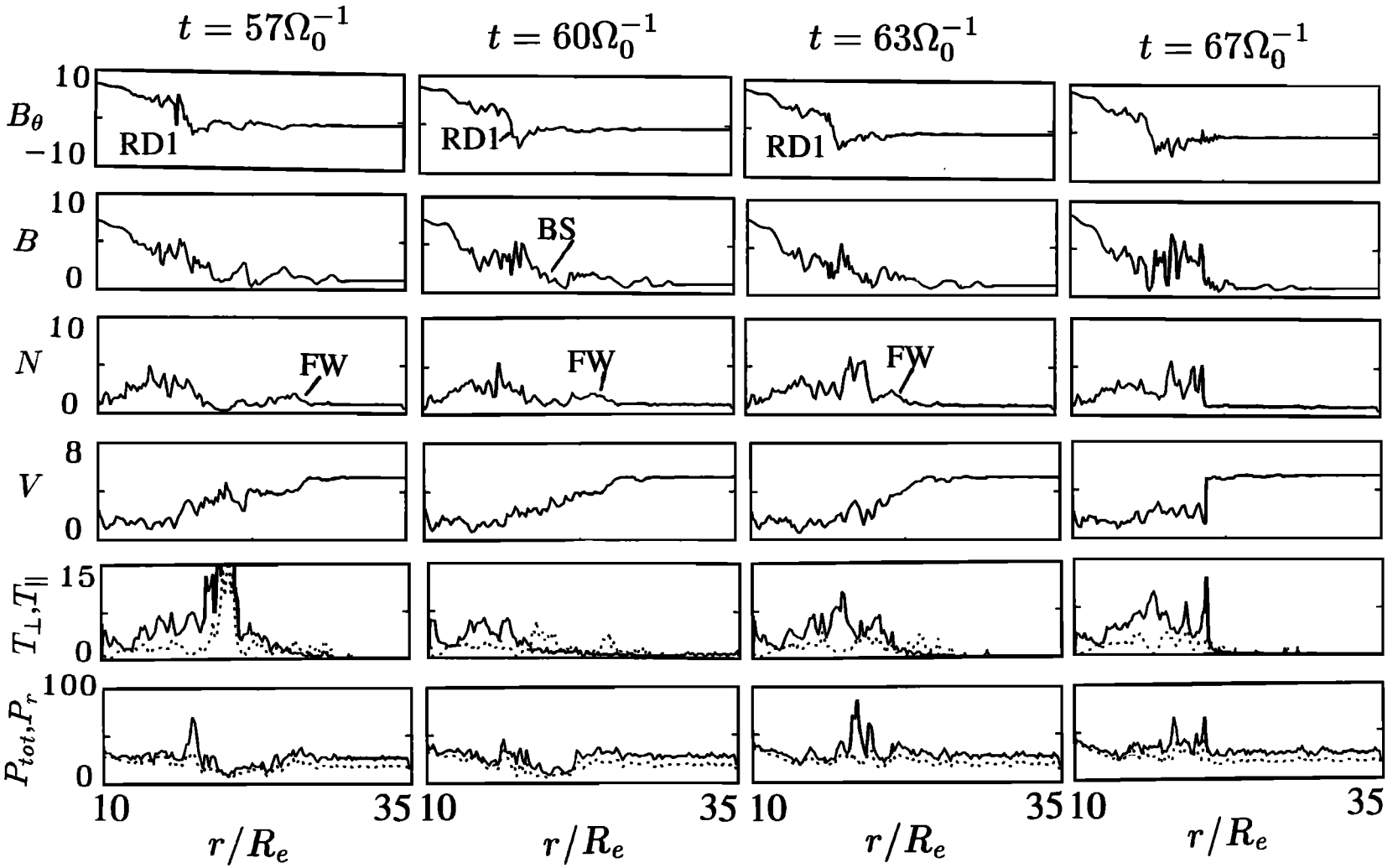

Figure 10. Spatial profiles of B_θ, B, N, V, $T_\perp$ (solid lines), $T_\parallel$ (dotted lines), P_{tot} (solid lines), and P_r (dotted lines) for case 3 along $\theta = 45^o$ in a time sequence from $t = 57$ to $67\Omega_0^{-1}$.

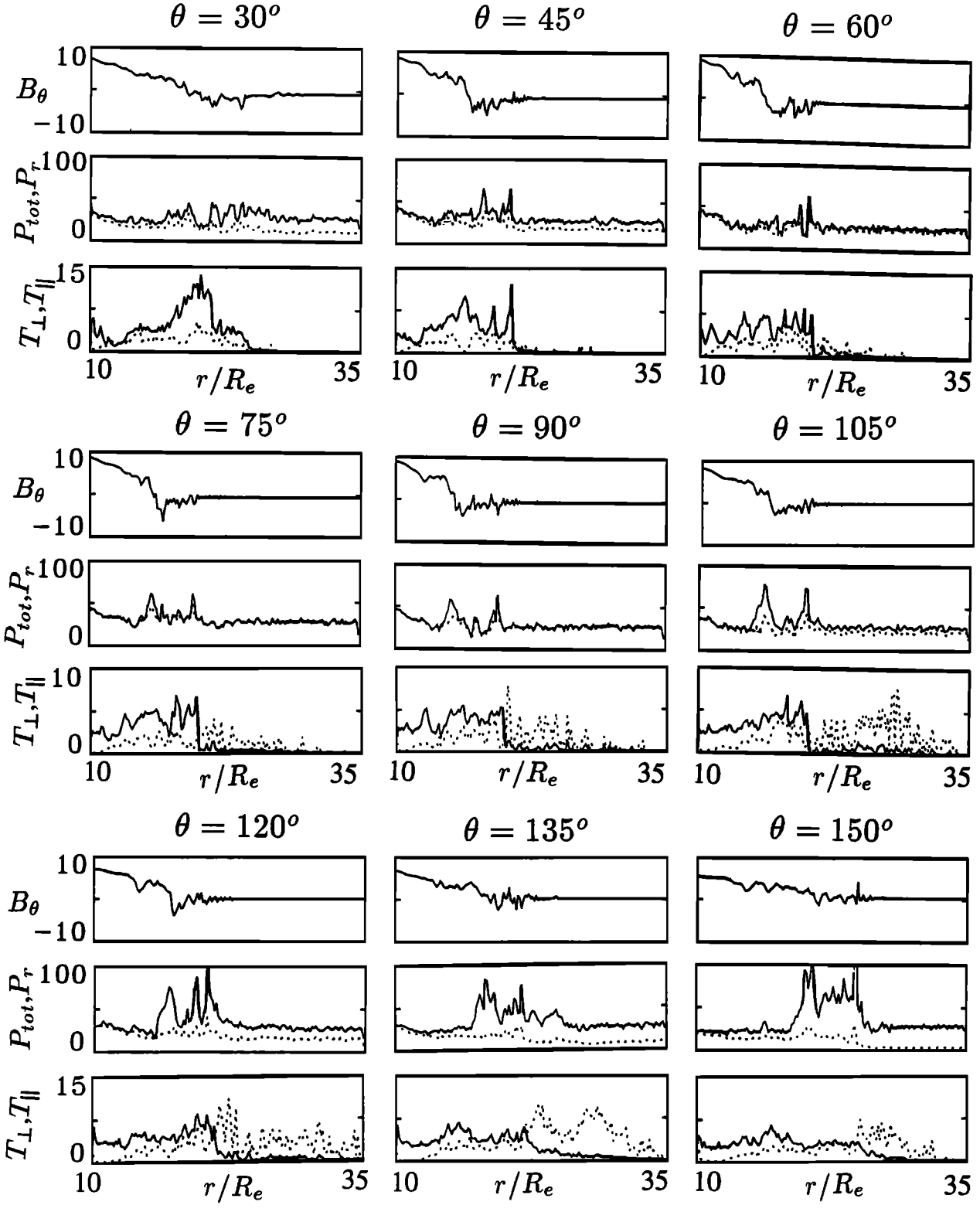

Figure 11. Results of case 3: spatial profiles of physical quantities at various local times when the pressure pulse propagates to a middle position between the bow shock and the magnetopause, at $t \sim 67\text{-}70\Omega_0^{-1}$.

BS/RD interaction, similar to the 1-D results and consistent with the MHD simulation by *Yan and Lee* [1994]. The shape of the 2-D bow shock front may be modified. This pressure pulse is mainly due to the increase in the dynamic pressure. In the subsolar region the increase in P_r at the pressure pulse may be much smaller than that in P_{tot}, where $P_r = (P + B^2/2\mu_0 + m_i N V_r^2)$ is the total pressure associated with the radial component, which

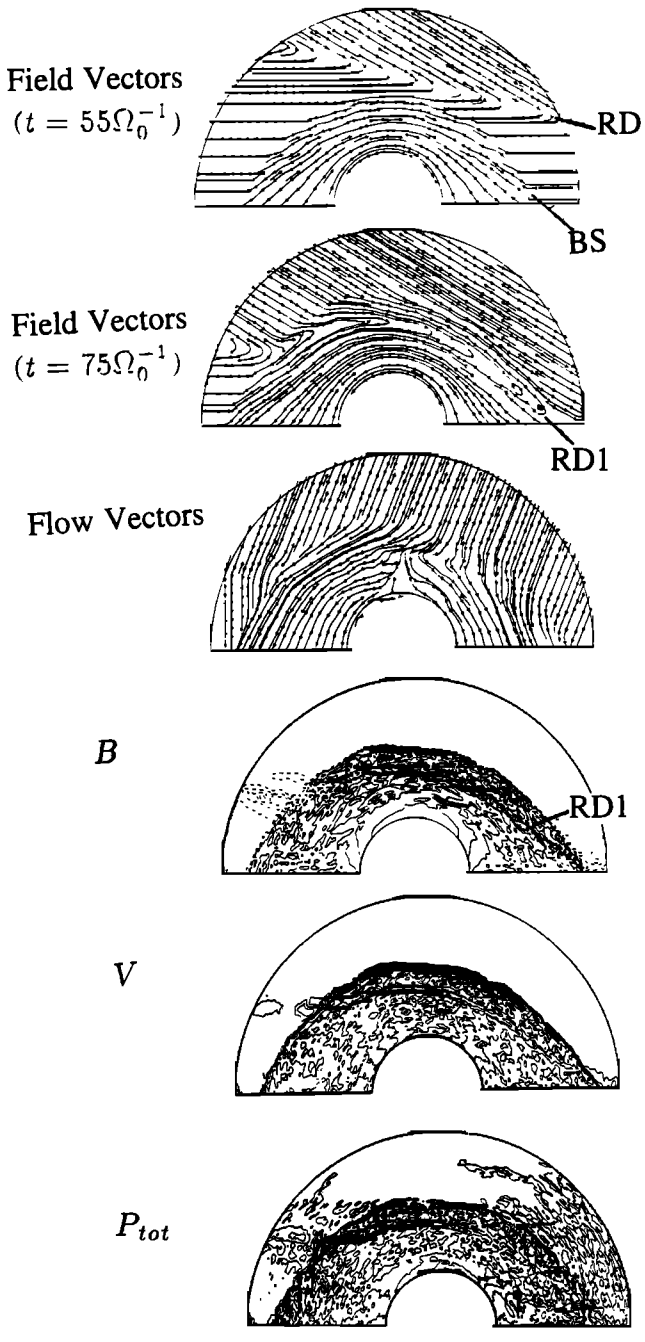

Figure 12. Results of case 4: (top) magnetic field vectors at $t = 55\Omega_0^{-1}$ and (two through six) field vectors, flow vectors, and contours of B, V, and P_{tot} at $t = 75\Omega_0^{-1}$, respectively. The propagation direction of RD has an angle of 15^o from the $-x$ axis.

is in the normal direction of the magnetopause, of flow velocity. This occurrence is due to the fact that the normal flow speed is nearly constant across RD1. The substantial increase in the dynamic pressure NV^2 is mainly caused by the deflection of the flow tangential to the bow shock normal direction, which is nearly proportional to the change of magnetic field across RD1. The pressure pulse propagates to the magnetopause nearly with the intermediate mode speed. At the locations away from the subsolar point, however, the plasma flow parallel to the RD1 front may have a normal component at the magnetopause. The total pressure P_r may thus be moderate. Nevertheless, the strength of pressure pulses at the dawnside and duskside is in general asymmetric.

3. In addition, reflected ions at the bow shock may generate pressure pulses in the upstream region when IMF changes its direction. In the 2-D simulation a local quasi-parallel bow shock may become a quasi-perpendicular shock while an interplanetary rotational discontinuity propagates to the bow shock. The reflected ions then move back to the quasi-perpendicular shock. As a result a pressure pulse with positively correlated variations in magnetic field, plasma density, dynamic pressure, and total pressure is present in the foreshock. This pressure pulse convects through and interacts with the bow shock, producing a pressure pulse in the downstream region. This pressure pulse quickly propagates to the magnetopause with magnetosonic speed. It can catch up to the pressure pulse due to RD1.

The interaction of the pressure pulses with the magnetopause is not simulated in this study. As the pressure pulse associated with RD1 approaches the magnetopause, it may be deflected and slowed, and an enhanced thermal and magnetic pressure is applied to the magnetosphere. In the 2-D MHD simulation by *Yan and Lee* [1994] for the generation of slow mode structure in front of the magnetopause they found that the intermediate and slow modes generated by the RD/BS interaction can stay in front of the magnetopause for about 15 min. The manner of the interaction between this pressure pulse and the magnetosphere, however, remains to be solved. On the other hand, the upstream pressure pulses generated by reflected ions while IMF changes direction may have a spatial length of several earth radii, corresponding to a duration of a few minutes, as spacecraft may see in the upstream. Unlike the pressure pulse associated with RD1, the downstream pressure pulse produced by this upstream wave can hit the magnetopause, having a direct interaction with the magnetosphere. The simulation study by *Mandt and Lee* [1991] indicates that downstream fast waves can pass through the magnetopause and generate Pc 1 waves and thus magnetospheric compressions. While large-amplitude pressure pulses have been found upstream of the bow shock and a correspondence between these upstream pressure variations and magnetospheric compressions has also been frequently observed [e.g., *Fairfield et al.*, 1990], a complete search for the pressure pulses in the magnetosheath when the IMF varies has not been reported.

In our simulation it is found that the overall amplitude of the pressure pulses in P_{tot} can be up to 100% of the background magnetosheath value. The increase in P_r may take a fraction of this strength. It should be pointed out, however, that this strength of the pressure pulses obtained from the 2-D simulation may be overestimated. A better estimate for the properties of the pressure pulses may be obtained by conducting three-dimensional simulations.

It is expected that the pressure pulses impinging on the magnetopause may compress the magnetopause globally, cause the wavy motion of the magnetopause, and generate antisunward propagating ripple. Other studies [e.g., *Friis-Christensen et al.*, 1988; *Sibeck et al.*, 1989; *Lysak et al.*, 1994] have suggested that pressure pulses can contribute to the observed ionospheric traveling vortices and lead to the magnetic impulse events observed in the polar ionosphere. The statistical study by *Konik et al.* [1994] shows that over 50% of the observed MIEs are accompanied by variations in the IMF direction. In line with this observation our simulation study also suggests that variations in the IMF direction may lead to pressure pulses at the magnetopause and thus the observed MIEs at high latitudes.

Acknowledgments. This work was supported by ONR grant NAVY-N00014-951-0839 to Auburn University, AFOSR grant F49620-94-0218 to the University of Alaska, and a grant from the National Science Council to the National Cheng Kung University. Computer resources were provided by the San Diego Supercomputer Center and the Arctic Region Supercomputer Center.

The Editor thanks D. Winske and another referee for their assistance in evaluating this paper.

References

Bering, E. A., III, J. R. Benbrook, G. J. Byrne, B. Liao, J. R.. Theall, L. J. Lanzerotti, C. G. Maclennon, A. Wolfe, and G. L. Siscoe, Impulsive electric and magnetic field perturbations observed over South Pole: Flux transfer events?, *Geophys. Res. Lett., 15*, 1545, 1988.

Bering, E. A., III, L. J. Lanzerotti, J. R. Benbrook, and Z.-M. Lin, Solar wind properties observed during high-latitude impulsive perturbation events, *Geophys. Res. Lett., 17*, 579, 1990.

Burgess, D., Cyclic behavior at quasi-parallel collisionless shocks, *Geophys. Res. Lett., 16*, 345, 1989.

Cahill, L. J., and V. L. Patel, The boundary of the geomagnetic field, August to November 1961, *Planet. Space Sci., 15*, 997, 1967.

Crooker, N. U., T. E. Eastman, and G. S. Stiles, Observation of plasma depletion in the magnetosheath at the dayside magnetopause, *J. Geophys. Res., 84*, 869, 1979.

Denton, R. E., S. P. Gary, X. Li, B. J. Anderson, J. W. LaBelle, and M. Lessard, Low-frequency fluctuations in the magnetosheath near the magnetopause, *J. Geophys. Res., 100*, 5665, 1995.

Fairfield, D. H., W. Baumjohann, G. Paschmann, H. Luhr, and D. G. Sibeck, Upstream pressure variations associated with the bow shock and their effects on the magnetosphere, *J. Geophys. Res., 95*, 3773, 1990.

Farrugia, C. J., M. P., Freeman, S. W. H. Cowley, D. J. Southwood, M. Lockwood, and A. Etemadi, Pressure-driven magnetopause motions and attendant response on the ground, *Planet. Space Sci., 37*, 589, 1989.

Friis-Christensen, M., A. McHenry, C. R. Clauer, and S. Vennerstrom, Ionospheric traveling convection vortices observed near the polar cleft: A triggered response to sudden change in the solar wind, *Geophys. Res. Lett., 15*, 253, 1988.

Glassmeier, K.-H., and C. Heppner, Traveling magnetospheric convection twin vortices: Another case study, global characteristics, and a model, *J. Geophys. Res., 97*, 3977, 1992.

Glassmeier K.-H., M. Hoenisch, and J. Untiedt, Ground-based and satellite observations of traveling magnetospheric convection twin vortices, *J. Geophys. Res., 94*, 2520, 1989.

Greenstadt, E. W., and R. W. Fredricks, Shock systems in collisionless space plasmas, in *Solar System Plasma Physics*, Vol. III, edited by L. J. Lanzerotti, C. F. Kennel, and E. N. Parker, p. 3, North-Holland, Amsterdam, 1979.

Hassam, A. B., Transmission of Alfven waves through the Earth's bow shock: Theory and observation, *J. Geophys. Res., 83*, 643, 1978.

Kan, J. R., and D. W. Swift, Structure of the quasi-parallel bow shock: Results of numerical simulations, *J. Geophys. Res., 88*, 6919, 1983.

Kaufmann, R. L., and A. Konradi, Explorer 12 magnetopause observations: Large-scale nonuniform motion, *J. Geophys. Res., 74*, 3609, 1969.

Konik, R. M., L. J. Lanzerotti, A. Wolfe, C. G. Maclennan, and D. Venkatesan, Cusp latitude magnetic impulse events, 2, Interplanetary magnetic field and solar wind conditions, *J. Geophys. Res., 99*, 14,931, 1994.

Krauss-Varban, D., and N. Omidi, Structure of medium Mach number quasi-parallel shocks: Upstream and downstream waves, *J. Geophys. Res., 96*, 17,715, 1991.

Landau, L. D. and E. M. Lifshitz, *Electrodynamics of Continuous Media*, Pergamon, Tarrytown, N. Y., 1960.

Lanzerotti, L. J., Comment on "Solar wind dynamic pressure variations and transient magnetospheric signatures," *Geophys. Res. Lett., 16*, 1197, 1989.

Lanzerotti, L. J., L. C. Lee, C. G. Maclennan, A. Wolfe, and L. V. Medford, Possible evidence of flux transfer events in the polar ionosphere, *Geophys. Res. Lett., 13*, 1089, 1986.

Lanzerotti, L. J., R. D. Hunsucker, D. Rice, L. C. Lee, A. Wolfe, C. G. Maclennan, and L. V. Medford, Ionospheric and ground-based response to field-aligned currents near the magnetospheric cusp regions, *J. Geophys. Res., 92*, 7739, 1987.

Lee, L. C., M. Yan, and J. G. Hawkins, A study of slow mode structures in the dayside magnetosheath, *Geophys. Res. Lett., 18*, 381, 1991.

Lees, L., Interaction between the solar wind and the geomagnetic cavity, *AAIA J., 2*, 1576, 1964.

Leroy, M. M., and D. Winske, Backstreaming ions from oblique earth bow shocks, *Ann. Geophys., 1*, 527, 1983.

Leroy, M. M., D. Winske, C. C. Goodrich, C. S. Wu, and K. Papadopoulos, The structure of perpendicular bow shocks, *J. Geophys. Res., 87*, 5081, 1982.

Lin, Y., and L. C. Lee, Structure of the dayside reconnection layer in resistive MHD and hybrid model, *J. Geophys. Res., 98*, 3919, 1993.

Lin, Y., L. C. Lee, and M. Yan, Generation of dynamic pressure pulses downstream of the bow shock by variations in the interplanetary magnetic field orientation, *J. Geophys. Res., 101*, 479, 1996.

Lysak, R. L., Y. Song, and D.-H. Lee, Generation of ULF waves by fluctuations in the magnetopause position, in *Solar Sources of Magnetospheric Ultra-Low-Frequency Waves, Geophys. Monogr. Ser.*, Vol. 81, edited by M. J. Engebretson, K. Takahashi, and M. Scholer, p. 273, AGU, Washington, D. C., 1994.

Lyu, L. H., and J. R. Kan, Ion leakage, ion reflection, ion heating and shock-front reformation in a simulated supercritical quasi-parallel collisionless shock, *Geophys. Res. Lett., 17*, 1041, 1990.

Mandt, M. E., and L. C. Lee, Generation of Pc 1 waves by the ion temperature anisotropy associated with fast shocks caused by sudden impulses, *J. Geophys. Res., 96*, 17,897, 1991.

McKenzie, J. F., and K. O. Westphal, Interaction of hydro-

magnetic waves with hydromagnetic shocks, *Phys. Fluids., 13*, 630, 1970.

Russell, C. T., and R. C. Elphic, Initial ISEE magnetometer results: Magnetopause observations, *Space Sci. Rev., 22*, 691, 1978.

Scholer, M., and T. Terasawa, Ion reflection and dissipation at quasi-parallel collisionless shocks, *Geophys. Res. Lett., 17*, 119, 1990.

Sibeck, D. G., W. Baumjohann, and R. E. Lopez, Solar wind dynamic pressure variations and transient magnetospheric signatures, *Geophys. Res. Lett., 16*, 13, 1989.

Song, P., C. T. Russell, and M. F. Thomsen, Slow mode transition in the frontside magnetosheath, *J. Geophys. Res., 97*, 8295, 1992.

Southwood, D. J., and M. G. Kivelson, The magnetohydrodynamic response of the magnetospheric cavity to changes in solar wind pressure, *J. Geophys. Res., 95*, 2301, 1990.

Southwood, D. J., and M. G. Kivelson, On the form of the flow in the magnetosheath, *J. Geophys. Res., 97*, 2873, 1992.

Spreiter, J. R., and S. S. Stahara, Magnetohydrodynamic and gasdynamic theories for planetary bow waves, in *Collisionless Shocks in the Heliosphere: Reviews of Current Research, Geophys. Monogr., Ser.*, Vol. 35, edited by B. T. Tsurutani and R. G. Stone, pp. 85-107, AGU, Washington, D. C., 1985.

Swift, D. W., Use of a hybrid code to model the Earth's magnetosphere, *Geophys. Res. Lett., 22*, 311, 1995.

Swift, D. W., Use of a hybrid code for a global-scale plasma simulation, *J. Comput. Phys.*, in press, 1996.

Swift, D. W., and L. C. Lee, Rotational discontinuities and the structure of the magnetopause, *J. Geophys. Res., 88*, 111, 1983.

Thomas, V. A., D. Winske, M. F. Thomsen, and T. G. Onsager, Hybrid simulation of the formation of a hot flow anomaly, *J. Geophys. Res., 96*, 11,625, 1991.

Thomas, V. A., D. Winske, and M. F. Thomsen, Simulation of upstream pressure pulse propagation through the bow shock, *J. Geophys. Res., 100*, 23,481, 1995.

Wu, B. H., M. E. Mandt, L. C. Lee, and J. K. Chao, Magnetospheric response to solar wind dynamic pressure variations: Interaction of interplanetary tangential discontinuities with the bow shock, *J. Geophys. Res., 98*, 21,297, 1993.

Yan, M., and L. C. Lee, Generation of slow-mode waves in front of the dayside magnetopause, *Geophys. Res. Lett., 21*, 629, 1994.

Yan, M., and L. C. Lee, Interaction of interplanetary shocks and rotational discontinuities with the Earth's bow shock, *J. Geophys. Res., 101*, 4835, 1996.

Zwan, B. J., and R. A. Wolf, Depletion of solar wind plasma near a planetary boundary, *J. Geophys. Res., 81*, 1636, 1976.

Y. Lin, Department of Physics, Auburn University, 206 Allison Laboratory, Auburn, AL 36849-5311. (e-mail: ylin@physics.auburn.edu)

D. W. Swift, Geophysical Institute, University of Alaska, Fairbanks, AK 99775-7320.

L. C. Lee, Department of Earth Science, College of Science, National Cheng Kung University, Tainan, Taiwan.

(Received June 24, 1996; revised August 27, 1996;
accepted September 4, 1996.)